

Solid-State Nanopores with Atomically Smooth Surface for ssDNA Transport

Alex Smolyanitsky*

Applied Chemicals and Materials Division, National Institute of Standards and Technology, Boulder, CO 80305, USA

Binquan Luan†

IBM Thomas J. Watson Research Center, 1101 Kitchawan Road, Yorktown Heights, NY, 10598, USA

(Dated: April 4, 2022)

Engineered protein nanopores have been demonstrated to be promising candidates for *de-novo* high-throughput, low-cost DNA sequencing. Their solid-state analogs, on the other hand, remain lacking for this application due to poorly controllable surface structures and nonspecific nucleotide-nanopore interactions. Resolving these challenges is key to achieving reliable detection of nucleotide-specific electrical signals in nanoscale DNA readers. Here, using density functional theory calculations, we demonstrate that nanopores in bilayer hexagonal boron nitride possess an atomically smooth surface, seamlessly connecting the two stacked hexagonal lattices. Using all-atom molecular dynamics simulations, we demonstrate low-friction electrophoretic transport of aqueous ssDNA through such bilayer-hBN nanopores. We unveil the fundamental mechanisms underlying the observed continuous ssDNA transport across these pores and explain why they present a more favorable environment for ssDNA transport in comparison with monolayer hBN-based nanopores featuring abrupt or disordered edges.

Nanopore-based sensing of DNA nucleotides is becoming essential to human genome sequencing [1] and the recently proposed DNA storage technologies [2]. After decades of extensive studies, protein-nanopore-based DNA sequencing is poised to become a low-cost, high-throughput complement or possibly replacement for the existing technologies, including the now-ubiquitous dye sequencing [3] and the Sanger method [4]. In the meantime, the use of solid-state nanopores (nanoscale orifices in thin SiO_2 or Si_3N_4 membranes) for sequencing remains challenging. Despite significant merits, such as chemical and mechanical robustness, solid-state nanopores suffer several serious drawbacks that limit their application. For example, a typical solid-state nanopore drilled with a focused electron or ion beam usually has poorly controllable geometric and surface properties (such as hydrophobicity and charge density). Consequently, the pore-to-pore variation in these properties limits the reliability of measured electrical currents used in sequencing and ultimately reduces detection accuracy [5, 6]. In order to achieve solid-state nanopores with well-defined atomic structures similar to the ones in transmembrane proteins, various two-dimensional (2D) materials have been proposed as host membranes [7–10]. In particular, electrophoretic transport of DNA through graphene- and hexagonal boron nitride (hBN)-based nanopores has been studied extensively. So far, most cases of successful transport were demonstrated with double-stranded DNA (dsDNA) [7, 9, 10]. Transport of single-stranded DNA (ssDNA), especially useful for sequencing, however, has proven to be more difficult in experiments [11]. Recent advances in fabrication have yielded atomically sculpted nanopores in molybdenum disulfide (MoS_2) monolayers, enabling a well-controlled pore geometry [12]. Nevertheless, continuous transport of a long ssDNA molecule

through nanopores in 2D nanosheets remains challenging due to fundamental limitations arising from non-specific adsorption of DNA bases in and around nanopores, causing pore clogging. In addition, pores in 2D-membranes are atomically thin, presenting an atomically sharp discontinuity for ssDNA adsorbed on a 2D nanosheet to traverse during its movement from one surface of the sheet to the other. In order to overcome this limitation, here we propose a nanopore with an atomically defined toroidal surface, which facilitates relatively low-friction (resulting from a low energy barrier) transport of ssDNA through an atomically thin membrane.

Previously, we studied nanopores in 2D heterostructures formed by stacking a graphene monolayer upon an MoS_2 monolayer [13]. Although nanopores in such heterostructures have a finite height, the complexity of interlayer interactions limits the overall promise in achieving predictable pore edge properties. Here, we investigate the edge surface of a hexagonal nanopore in an AA'-stacked hBN bilayer. Using density functional theory (DFT) calculations, we show that the optimized structure of such a pore features covalent B-N fusing between layers, resulting in an atomically smooth toroidal edge. Using density functional theory molecular dynamics (DFTMD), we demonstrate that the pore structure is stable at room temperature. Finally, using all-atom molecular dynamics (MD) informed by our DFT calculations, we demonstrate that an ssDNA molecule can be electrophoretically driven across this nanopore at a low biasing voltage. For comparison, this process is shown to be impossible in an identical system, except featuring a similarly sized pore in *monolayer* hBN. From analyzing the transport dynamics and energetics, we demonstrate nonequilibrium low-friction sliding of ssDNA through hBN bilayer-based nanopores, in contrast with asperity-like (high-friction)

ssDNA transport through an hBN-monolayer-based pore.

The ssDNA translocation results presented here were obtained using all-atom molecular dynamics (MD) simulations. The simulation cell was a 6-nm-tall hexagonal prism (cell vectors defined by $a = b = 5$ nm, $c = 6$ nm, $\alpha = \beta = 90^\circ$, $\gamma = 60^\circ$), containing the hBN membrane, a single strand of poly(dT₂₀), and an explicit aqueous 0.5M KCl solution (a total of ~ 16000 particles), as shown schematically in Figs. 1a (monolayer hBN) and 3a (bilayer hBN). Periodic boundaries were imposed in the XYZ -directions, which included a periodic ssDNA molecule similar to our earlier work [14, 15]. The ssDNA molecule was sized appropriately so as to freely adsorb on both sides of the membrane, resulting in roughly 12 nucleotides adsorbed on its *cis* side. The DNA model was AMBER-based [16], while the water model was TIP4P [17, 18]. The non-bonded portion of the nanoporous hBN models was set up within the AMBER framework according to recent work [19]. The membrane atoms were harmonically restrained in the XYZ -directions (spring constant of 500 N/m) around their equilibrium positions, which were obtained from the DFT calculations (see below). All MD simulations were carried out using the GPU-accelerated Gromacs 2018.1 software [20, 21]. Before production simulations, all systems were subject to at least 10 ns of relaxation in a semi-isotropic (cell size constant in-plane) NPT relaxation at $T = 300$ K and $P = 0.1$ MPa with a time-step of 1 fs. All production simulations were carried out in the NVT ensemble ($T = 300$ K) using a time-step of 2 fs. Unless stated otherwise, all DNA translocations across the pores were initiated by a uniform external electric field E , which we report in the form of effective transmembrane voltage $V = E \times h$, where $h = 6$ nm is the cell height. The assignment of atomic charges and equilibrium positions used in our MD simulations was obtained using DFT set-ups according to earlier work [19] (see details below). All porous membranes underwent static geometry optimization using large-scale DFT to obtain the equilibrium atomic positions and partial charges, which were then transferred directly into the MD setups. Note that the starting structure of the bilayer-based nanopore *did not feature any covalent B-N bonding* between the layers, similar to a system studied earlier [22]. The DFT calculations were set up with Perdew, Burke and Ernzerhof (PBE) exchange functional [23], Gaussian plane-wave pseudopotentials [24], and DZVP basis sets for boron and nitrogen atoms [25]. The total electric charge of all optimized structures was set to zero. The partial atomic charges were calculated using the Blöchl scheme [26] and directly transferred into the corresponding MD setups. The ground-state DFTMD simulations to test room-temperature stability of the fused bilayer-based pore were carried out for 1 ps in vacuum (NVT ensemble, $T = 300$ K maintained using a velocity-rescaling thermostat) with a time step of 1 fs. All DFT computations were performed

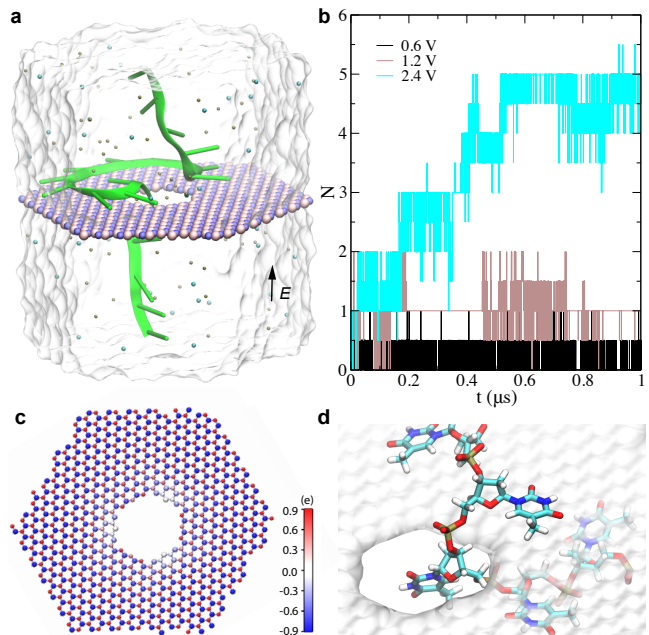


FIG. 1: ssDNA transport through a nanopore in an hBN monolayer. a) MD-simulated system. The ssDNA (colored in green) is in the cartoon representation; boron and nitrogen atoms in the membrane are shown as pink and blue spheres respectively; in the solution, K^+ and Cl^- ions are in tan and cyan respectively, and water is shown as a transparent surface. b) Cumulative flux of ssDNA *vs* time at various bias voltages. c) Charge distribution of all membrane atoms. d) A snapshot of ssDNA near the monolayer-based nanopore at $V=0.6$ V. The hBN membrane is in the molecular surface representation, while the ssDNA molecule is in the stick representation.

using the CP2K software package [27].

The results for ssDNA translocation across a hexagonal pore in monolayer hBN are provided in Fig. 1b, where cumulative fluxes of nucleotides are shown as a function of simulated time for various values of V . Importantly, we observe the presence of a threshold biasing voltage, below which ssDNA transport appears to be disallowed. From Fig. 1b, for the biasing voltages of 0.6V and 1.2V, ssDNA transport does not occur, *i.e.*, the ssDNA molecule is effectively trapped in the pore region, suggesting a significant transport-opposing barrier. This barrier is overcome at $V=2.4$ V when the vertical electrostatic force acting upon the negatively charged phosphate groups of the ssDNA is sufficient to essentially defeat static friction in the system. Interestingly, during the transport process, the ssDNA underwent a ratchet-like motion and transited the pore nucleotide-by-nucleotide (see steps in Fig. 1b).

From the simulated trajectories, we discovered the trapped state of ssDNA during transport as shown in Fig. 1d. Namely, a nucleotide resides inside the nanopore desorbed from the membrane edge and surrounded by water, while the two neighboring nucleotides ahead and behind remain adsorbed on the *trans* and *cis* sides of

the hBN monolayer, respectively. This suggests that upon translocation a nucleotide must first desorb from the *cis* hBN surface, enter the water environment inside the pore (Fig. 1d), and finally readsorb on the *trans* side. This transition is expected to impose barriers associated with desorption and redistributing water surrounding the pore edge. It is worth mentioning that field-induced desorption throughout the ssDNA-hBN contact may assist translocation at very high biases. Given the thinness of hBN and the fact that most of the bias voltage drops across the membrane, at $V=2.4$ V, the electric field perpendicular to the hBN surface is high (of order several V/nm). Therefore, in addition to acting upon the negatively charged phosphate groups in the ssDNA, this field is strong enough to reorient the adsorbed ssDNA bases from being parallel to the membrane surface to a perpendicular orientation aligned with the normal electric field. One may estimate the required biasing voltage V for thymine (T) using the equation $\vec{p} \cdot \vec{E} = \Delta F$, where \vec{p} (~ 4.4 Debye) is the dipole moment, \vec{E} the electric field inside the pore and ΔF the binding free energy for a nucleotide T moving from the bulk water to the hBN surface. Estimated from a previous study [13] we assume that ΔF is about 33 kJ/mol and $E=V/L$, where L is the effective thickness of the hBN monolayer (~ 0.4 nm). Thus, $V=\Delta FL/p$ and the predicted value is about 1.6 V, of the same order as the 2.4 V bias applied above. However, it is key that such voltages are exceedingly high for an experimental system, especially given the dielectric breakdown of hBN [28]. Therefore, our simulation results revealed why experimental observation of continuous ssDNA transport through nanopores in hBN or graphene monolayers has remained challenging.

As described above, the atomically sharp edge present in the monolayer-based nanopore produces an effective discontinuity between the surfaces of the membrane, which requires an ssDNA nucleotide to desorb into water inside the pore as a transition state. One may view this discontinuity as incompatible with the finite flexibility of ssDNA, effectively presenting the latter with a contact asperity. To investigate a case where this asperity is reduced significantly, we consider the proposed bilayer-based nanopore with a finite height of ~ 0.8 nm. Figure 2a shows the top view of the bilayer hBN nanopore, provided with a slight tilt to show that the positions of N and B atoms correspond to an AA' stack.

Upon DFT optimization of the bilayer-based system (containing a total of 1492 atoms and 5968 electrons) described above, remarkably, interlayer B-N covalent bonds formed at the nanopore surface, as shown in Figs. 2b (tilted top view) and 2c (side view). Namely, for a pair of B and N atoms on top of each other at the pore edge, the distance between them gradually decreased from 0.34 nm to 0.145 nm, corresponding to a strained covalent B-N bond. A total of 18 new B-N bonds were formed, symmetrically distributed throughout the pore surface.

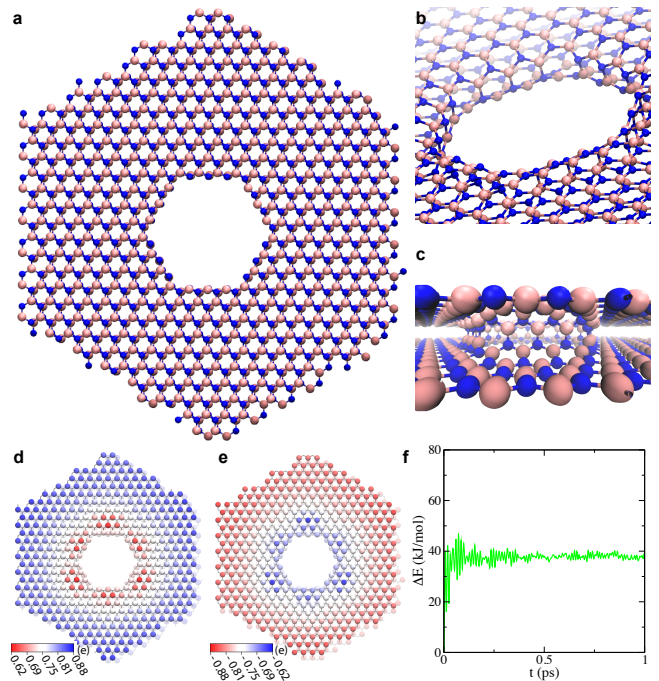


FIG. 2: DFT-based calculations for the nanopore in an hBN bilayer. a) Top view of the porous membrane. b) Tilted and enlarged view of the pore area (after static optimization). c) Side and perspective views of the post-optimization pore region. d) Charge distribution of all B atoms. e) Charge distribution of all N atoms. f) Change in potential energy of the system as a function of time as obtained in a DFTMD simulation ($T=300$ K), relative to the starting atomic configuration.

Consequently, the lattices in each layer were strained, overall resulting in a smooth toroidal-like inner surface of the pore (Figs. 2b,c). Accompanied by this restructuring, the partial atomic charges near the pore were $Q_B = +0.62e$ and $Q_N = -0.62e$, reduced from the bulk hBN values of $Q_B^{\text{bulk}} = +0.9e$ and $Q_N^{\text{bulk}} = -0.9e$ [19] (see charge distributions in Fig. 2d,e). Much more importantly, the electron density distribution at the edge naturally inherited the polarity-alternating pattern of bulk hBN (neutral over the BN unit cell). This charge distribution is unlike that for the monolayer-based pore, which possesses radially dipolar edges exposed to water (see Fig. 1c). As will be shown later, this edge is surrounded by a considerably more stable hydration shell.

In order to assess the stability of the bilayer-based fused pore, we carried out room-temperature DFTMD simulations, as described above. From the simulated trajectories we observed that the nanopore remained stable with its fused surface intact. Figure 2f shows that the potential energy of the system increased by $\Delta E \sim 37.6$ kJ/mol from that corresponding to the starting statically optimized structure. Note that ΔE remained nearly constant after settling within the first 0.5 ps of the DFTMD simulation.

After feeding the structure and the corresponding atomic charges from the DFT calculations into the clas-

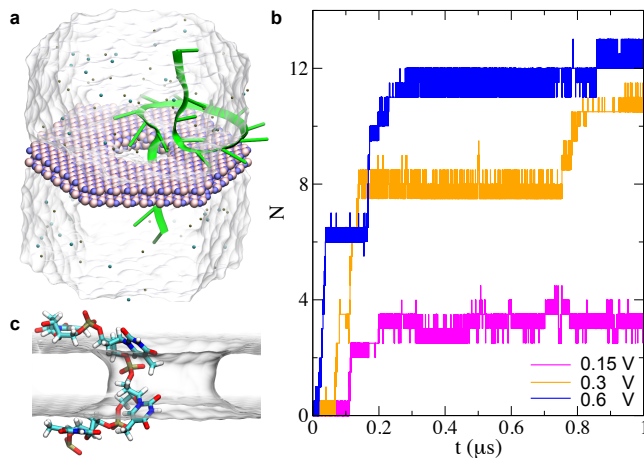


FIG. 3: ssDNA transport through a nanopore in an hBN bilayer. a) MD simulation system. The illustration scheme is identical to that in Figure 1. b) Cumulative flux of ssDNA *vs* time at various bias voltages. c) A snapshot of ssDNA near the pore at $V=0.6$ V. The bilayer hBN membrane is in the molecular surface representation, while the ssDNA molecule is in the stick representation.

sical MD setup, we simulated aqueous ssDNA translocation through the bilayer-based nanopore. Figure 3a shows the simulated system. After the initial equilibration without a biasing field, the majority of nucleotides resided on the *cis* surface of the hBN bilayer. At a biasing voltage of 0.6 V, the ssDNA molecule translocated through nanopore in about 0.3 μ s. Note that due to the periodic set-up of the ssDNA molecule, among the total of 20 nucleotides in the ssDNA molecule, only 12 of them initially resided on the *cis* surface and could transit the pore, while the remaining eight remained in water. Therefore, in the presented simulation, a total of 12 nucleotides could transit the pore, as confirmed in Fig. 3b.

At a lower bias of 0.3 V, the ssDNA molecule remained able to transit the pore, but the overall transport speed was reduced 3-4 times. At an even lower bias of 0.15 V, we observed translocation of only three nucleotides within the simulated time, which suggests that the critical bias is around 0.15 V, *an order of magnitude lower than that for the monolayer-based pore* (2.4 V). It is noteworthy that the transport dynamics here is reminiscent of the stick-slip process ubiquitous in tribology, with many plateaus in Fig. 3b corresponding to the "stick" state and thermally-activated transitions corresponding to slipping events [29–33].

As shown in Fig. 3c, during transport, *ssDNA nucleotides remained adsorbed on the smooth surface of the pore edge*, because the curvature of the toroidal edge of the pore is now compatible with the flexibility of ssDNA. However, as will be shown later, even in the event of transient desorption, given the bulk-like edge electrostatics, the surrounding water layer is considerably less stable than that around the monolayer-based pore. The same may in fact be true in comparison with any pore with

water-exposed locally charged edges. As described, a combination of nanomechanical compatibility and considerably lower solvation/desolvation energy cost reduces the local contact asperity described for the monolayer case and enables continuous, relatively low-friction transport of ssDNA. For a more quantitative analysis, we resumed *unbiased* MD simulations of both the monolayer- and bilayer-based pores (starting with ssDNA conformations shown in Figs. 1d and 3c, respectively). For the bilayer-based pore, the region of ssDNA spanning the pore (including the nucleotides adsorbed above and below edge) remained continuously adsorbed and corresponding to Fig. 3c. From a 40-ns-long MD simulation, we obtained the average potential energies between each nucleotide and the entire hBN bilayer, shown in Fig. 4. The two nucleotides inside the pore are labeled B_0 and B_1 ; the two nucleotides on the *cis* side of the bilayer are labeled as B_{-2} and B_{-1} ; the two nucleotides on the *trans* side are labeled as B_2 and B_3 . The results in Fig. 4 illustrate that for all nucleotides in the vicinity of the bilayer-based pores had comparable interaction energies for all nucleotides, *i.e.*, confirming that nucleotide-edge interaction is similar to that between a nucleotide and bulk hBN. A similar calculation for the monolayer-based pore reveals a different situation. As shown in Fig. 4, the mean interaction energy for the nucleotide inside the pore (Fig. 1d) is significantly smaller (less negative) than those for nucleotides on the *cis* and *trans* surfaces of hBN, confirming desorption proposed earlier as one of the underlying causes for the transport-opposing barrier.

Finally, we assessed the stability of the water shell in the vicinity of the pores. As obtained from the unbiased MD simulations, the average energy of interaction between water and the entire pore region was -605.7 ± 8.6 kJ/mol and -488.2 ± 6.9 kJ/mol for the monolayer and bilayer case, respectively. The energy difference of almost 120 kJ/mol supports our hypothesis of a larger energy barrier associated with water displacement near the pore edge by nucleotides traversing a monolayer-based pore, compared with the bilayer-based pore.

In summary, we have proposed an hBN-bilayer-based nanopore, which possesses a toroidal bulk-like edge surface without dangling bonds, seamlessly connecting the two surfaces of the host membrane. This nanopore is also shown to feature a bulk-hBN-like electron density distribution at its edge. Together, the smooth geometry and the favorable electrostatic environment enable continuous ssDNA transport under electric bias. Specifically, we demonstrated that low-friction transport becomes possible due to significant reduction of the desorption- and solvation-related barriers at the pore edge, in comparison with a monolayer-based nanopore. A similar advantage may be possible in comparison with a multitude of nanopores featuring disordered edges. Given that an ssDNA molecule is generally adsorbed on a 2D nanosheet [10, 34] before transport becomes possible, a

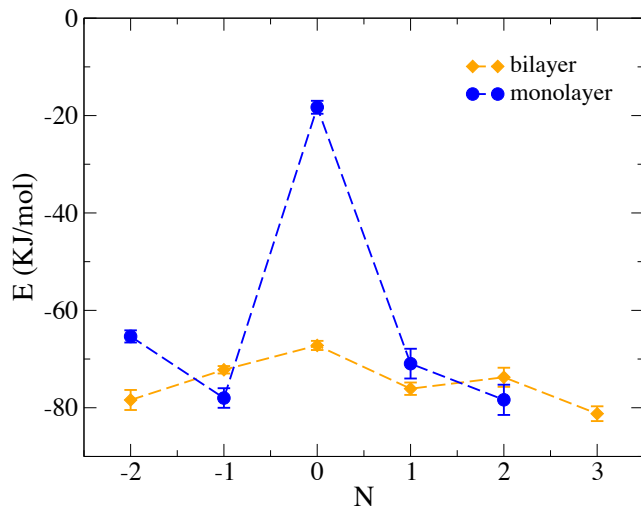


FIG. 4: Potential energy of interaction between ssDNA nucleotides and the pore vicinity for monolayer hBN (blue) and bilayer hBN (orange).

pore featuring bulk-like edges appears to be a highly attractive feature for ssDNA transport. It is worth mentioning that similarly structured pores with may also be possible in AA-stacked graphene bilayers. Overall, we presented a solid-state nanopore with a smooth and well-defined atomic structure, potentially paving the way toward achieving continuous electrophoretic DNA transport in solid-state nanopores and making nanoscale solid-state DNA readers a reality.

ACKNOWLEDGMENTS

B.L. gratefully acknowledges the financial support from the IBM Bluegene Science Program. A.S. gratefully acknowledges support from the Materials Genome Initiative.

REFERENCES

-
- * Corresponding author: alex.smolyanitsky@nist.gov
† Corresponding author: bluan@us.ibm.com
- [1] D. Deamer, M. Akeson, and D. Branton, **34**, 518 (2016).
 - [2] V. Zhirnov, R. M. Zadegan, G. S. Sandhu, G. M. Church, and W. L. Hughes, *Nat. Mater.* **15**, 366 (2016).
 - [3] D. R. Bentley, S. Balasubramanian, H. P. Swerdlow, G. P. Smith, J. Milton, C. G. Brown, K. P. Hall, D. J. Evers, C. L. Barnes, H. R. Bignell, et al., *Nature* **456**, 53 (2008), ISSN 1476-4687.
 - [4] F. Sanger, S. Nicklen, and A. Coulson, *Proc. Nat. Acad. Sci. USA* **74**, 5463 (1977).
 - [5] S. Carson and M. Wanunu, *Nanotechnology* **26**, 074004 (2015).
 - [6] D. Branton, D. W. Deamer, A. Marziali, H. Bayley, S. A. Benner, T. Butler, M. Di Ventra, S. Garaj, A. Hibbs, X. Huang, et al., *Nature Biotechnology* **26**, 1146 (2008), ISSN 1546-1696.
 - [7] S. Garaj, W. Hubbard, A. Reina, J. Kong, D. Branton, and J. A. Golovchenko, *Nature* **467**, 190 (2010), ISSN 1476-4687.
 - [8] D. B. Wells, M. Belkin, J. Comer, and A. Aksimentiev, *Nano Letters* **12**, 4117 (2012), ISSN 1530-6984.
 - [9] G. F. Schneider, S. W. Kowalczyk, V. E. Calado, G. Pandraud, H. W. Zandbergen, L. M. K. Vandersypen, and C. Dekker, *Nano Letters* **10**, 3163 (2010), ISSN 1530-6984.
 - [10] C. A. Merchant, K. Healy, M. Wanunu, V. Ray, N. Patterman, J. Bartel, M. D. Fischbein, K. Venta, Z. Luo, A. T. C. Johnson, et al., *Nano Letters* **10**, 2915 (2010), ISSN 1530-6984.
 - [11] S. Garaj, S. Liu, J. A. Golovchenko, and D. Branton, *Proc. Nat. Acad. Sci. USA* **110**, 12192 (2013).
 - [12] J. Feng, K. Liu, R. D. Bulushev, S. Khlybov, D. Dumcenco, A. Kis, and A. Radenovic, **10**, 1070 (2015).
 - [13] B. Luan and R. Zhou, *ACS Nano* **12**, 3886 (2018).
 - [14] E. Paulechka, T. A. Wassenaar, K. Kroenlein, A. Kazakov, and A. Smolyanitsky, *Nanoscale* **8**, 1861 (2016).
 - [15] A. Smolyanitsky, B. I. Jakobson, T. A. Wassenaar, E. Paulechka, and K. Kroenlein, *ACS Nano* **10**, 9009 (2016).
 - [16] W. D. Cornell, P. Cieplak, C. I. Bayly, I. R. Gould, K. M. Merz, Jr., D. M. Ferguson, D. C. Spellmeyer, T. Fox, J. W. Caldwell, and P. A. Kollman, **117**, 5179 (1995).
 - [17] H. W. Horn, W. C. Swope, J. W. Pitera, J. D. Madura, T. J. Dick, G. L. Hura, and T. Head-Gordon, *J. Chem. Phys.* **120**, 9665 (2004).
 - [18] J. Abascal, E. Sanz, R. García Fernández, and C. Vega, *J. Chem. Phys.* **122**, 234511 (2005).
 - [19] A. Govind Rajan, M. S. Strano, and D. Blankschtein, *The Journal of Physical Chemistry Letters* **9**, 1584 (2018).
 - [20] D. van der Spoel, E. Lindahl, B. Hess, G. Groenhof, A. E. Mark, and H. J. C. Berendsen, **26**, 1701 (2005).
 - [21] B. Hess, C. Kutzner, D. Van Der Spoel, and E. Lindahl, **4**, 435 (2008).
 - [22] B. Luan and R. Zhou, *Nano Lett.* (2019).
 - [23] J. P. Perdew, K. Burke, and M. Ernzerhof, *Phys. Rev. Lett.* **77**, 3865 (1996).
 - [24] C. Hartwigsen, S. Goedecker, and J. Hutter, *Phys. Rev. B* **58**, 3641 (1998).
 - [25] J. VandeVondele and J. Hutter, *The Journal of Chemical Physics* **127**, 114105 (2007).
 - [26] P. E. Blöchl, *The Journal of Chemical Physics* **103**, 7422 (1995).
 - [27] J. Hutter, M. Iannuzzi, F. Schiffmann, and J. VandeVondele, *WIREs Computational Molecular Science* **4**, 15 (2014).
 - [28] Y. Hattori, T. Taniguchi, K. Watanabe, and K. Nagashio, *ACS Nano* **9**, 916 (2015).
 - [29] B. Luan and M. O. Robbins, *Phys. Rev. Lett.* **93**, 036105 (2004).
 - [30] B. Luan, H. Peng, S. Polonsky, S. Rossnagel, G. Stolovitzky, and G. Martyna, *Phys. Rev. Lett.* **104**, 238103 (2010).
 - [31] A. Smolyanitsky, J. P. Killgore, and V. K. Tewary, *Phys.*

- Rev. B **85**, 035412 (2012).
- [32] A. Smolyanitsky and J. P. Killgore, Phys. Rev. B **86**, 125432 (2012).
- [33] A. Smolyanitsky, RSC Adv. **5**, 29179 (2015).
- [34] G. F. Schneider, Q. Xu, S. Hage, S. Luik, J. N. H. Spoor, S. Malladi, H. Zandbergen, and C. Dekker, Nature Communications **4**, 2619 (2013), ISSN 2041-1723.